Journal of Vacuum Science and Technology A

RESEARCH ARTICLE | MAY 16 2025

Atomic layer deposition of entropy stabilized $Zr_2Ta_2O_9$ and light activated self-rectifying resistive switching

Shane M. W. Witsell ; Konner E. K. Holden ; Dustin Z. Austin; John F. Conley, Jr.

J. Vac. Sci. Technol. A 43, 042402 (2025)
https://doi.org/10.1116/6.0004512

JVST A
Journal of Vacuum Science & Technology A

ARTICLE

pubs.aip.org/avs/jva

Atomic layer deposition of entropy stabilized $Zr_2Ta_2O_9$ and light activated self-rectifying resistive switching

Cite as: J. Vac. Sci. Technol. A 43, 042402 (2025); doi: 10.1116/6.0004512
Submitted: 21 February 2025 · Accepted: 28 April 2025 ·
Published Online: 16 May 2025

Shane M. W. Witsell,[1] Konner E. K. Holden,[2] Dustin Z. Austin,[2] and John F. Conley, Jr.[1,a)]

AFFILIATIONS

[1]School of Electrical Engineering and Computer Science, Oregon State University, Corvallis, Oregon 97331
[2]Lam Research, Tualatin, Oregon 97062

[a)]**Author to whom correspondence should be addressed:** jconley@eecs.oregonstate.edu

ABSTRACT

Ternary bulk $(A,B)_mO_{2m+1}$ materials, where A = Zr or Hf, B = Nb or Ta, and m is the multiplicity, were recently shown to be entropy stabilized at elevated temperature due to an exceptionally high degree of structural disorder. We report the transformation of atomic layer deposited amorphous ZrO_2–Ta_2O_5 thin films into ternary entropy stabilized $Zr_2Ta_2O_9$ upon annealing at 800 °C in N_2. Ag/$Zr_2Ta_2O_9$/Si metal/oxide/semiconductor devices exhibited light-activated self-rectifying resistive switching with a set field of ∼+0.56 MV/cm, a threshold field of +0.17 MV/cm, a reset field of −0.59 MV/cm, and a current ratio of 7000:1 between the low and high resistance states under illumination. Devices with unannealed (amorphous) films did not exhibit switching in this field range.

I. INTRODUCTION

Entropy stabilized oxides (ESOs), in which configurational entropy stabilizes the structure at high temperatures, were first reported by Rost *et al.* who used an equimolar mixture of five oxides (MgO, CoO, NiO, CuO, and ZnO) to make a single metastable phase material.[1] ESOs have since become a major area of research due to their potential for unique mechanical, refractory, catalytic, cryogenic, dielectric, enhanced cation solubility, and ion diffusion properties.[2–6] It had been generally thought that entropy stabilization required the homogeneous mixing of five or more elements in roughly equal atomic proportions.[1,7–10] Recent work, however, demonstrated entropy stabilization in ternary $A_6B_2O_{17}$ structures, a member of the homologous class $(A,B)_mO_{2m+1}$, where A = Zr or Hf, B = Nb or Ta, and m is the multiplicity.[11] The class of materials consisting of a mixture of AO_2 and B_2O_5 oxides has a maximum configurational entropy of $S_{config} = 4.5$ R J/mol K.[11] In the original work with bulk materials, stabilization of phase-pure ESO required extended (>10 h) annealing at temperatures between 1000 and 1400 °C.[6,12,13] The only reported $A_6B_2O_{17}$ thin films were deposited at 350 °C via RF magnetron sputtering.[14] The long range order in these materials reportedly imparts high relative permittivity, and recent reports have investigated the impact of doping.[14,15] As these materials show promising electrical properties, demonstrate resistive switching, and the constituent elements are nominally compatible with CMOS processing, it is advantageous to explore additional thin film deposition methods for ESO $A_6B_2O_{17}$ materials which may lend themselves to lower temperature stabilization. Atomic layer deposition (ALD) enables the deposition of highly uniform and conformal thin films on high aspect ratio structures, which is necessary for advanced CMOS fabrication. Of the possible $A_6B_2O_{17}$ perovskites, $Zr_6Ta_2O_{17}$ has been of interest for its high temperature phase stability and as a thermal insulator.[13] While ALD of ternary $Zr_xTa_yO_z$ and ZrO_2/Ta_2O_5 nanolaminate films and their capacitive and resistive switching properties have been investigated by several groups, none have reported synthesis of the ESO phase.[16–19] Most notably, Kukli *et al.* varied $ZrCl_4$ and $Ta(OEt)_5$ precursor pulse ratios with and without O_3 exposure to investigate ALD film growth, composition, and structure.[19] For a film deposited using alternating pulses of $Ta(OEt)_5$ and $ZrCl_4$, they saw crystallization upon annealing at 800 °C for 30 min in N_2 and identified a mixed phase, consisting of the $TaZr_{2.75}O_8$ (PDF-042-0060) ternary phase with an extra reflection from binary ZrO_2.[20]

In this work, we explore the stabilization of ALD deposited ZrO_2–Ta_2O_5 films into a member of the ESO $(A,B)_mO_{2m+1}$ homologous series via postdeposition annealing. In addition, we also report on light-activated self-rectifying resistive switching which was found to be unique to the ESO phase.

II. EXPERIMENT

ZrO_2–Ta_2O_5, ZrO_2, and Ta_2O_5 thin films were deposited in a PicoSun R150 hot wall ALD reactor at ~10 Torr using $ZrCl_4$ (99.5% purity) held at 165 °C, tantalum (V) ethoxide [$Ta(OEt)_5$] (99.98% purity) held at 55 °C, and ozone (O_3) as the oxidizing agent. O_3 was supplied using an IN-USA AC-2025 ozone generator operated at 50% power, resulting in an expected O_3/O_2 concentration of ~10%. To promote the homogeneous mixing of metal ions, a critical requirement for the ESO phase, ternary ZrO_2–Ta_2O_5 films were deposited at a chamber temperature of 250 °C using an "ABC" pulse sequence. In this method, O_3 is only pulsed once per ALD cycle, in contrast to a typical super-cycle in which O_3 would be pulsed twice, once after each metal precursor pulse.[19,21,22] Here, the "ABC" type ALD super-cycles were performed beginning with $ZrCl_4$, followed by $Ta(OEt)_5$, and finally, O_3 to fully oxidize and densify each layer. For comparison, binary oxide films were deposited at 250 °C by alternating the respective precursors with O_3. All films were deposited on p-type Si ($\rho = 0.016\ \Omega$ cm) to a target thickness of ~20 nm.

Film thickness was measured using a Film Sense FS1000 multiwavelength ellipsometer and Cauchy modeling. The crystal structure was assessed with grazing incidence x-ray diffraction (XRD) using a Rigaku SmartLab diffractometer. Postdeposition annealing of select samples was performed at 800 °C for 30 min in N_2 in a Neytech 9494401 vacuum muffle furnace. Rutherford backscattering spectrometry (RBS) was performed by EAG Laboratories using a 2.275 MeV He^{2+} ion beam energy at a backscattering angle of 160° and a grazing angle of ~100° with an estimated uncertainty in atomic percentage of ±0.5% for Zr and Ta and ±4% for O.

To investigate the resistive switching performance in both as-deposited and annealed ZrO_2–Ta_2O_5 films, metal/oxide/semiconductor (MOS) devices were formed by thermally evaporating 50 nm thick, 250 μm circular dot Ag contacts through a shadow mask using a VEECO 7700 thermal evaporator at 10^{-7} Torr. Electrical characterization was performed at room temperature on a probe station in a dark box. Contact with the p-Si bottom electrode was accomplished by gently scratching through the top surface of the 2.5×2.5 cm^2 coupon and soldering on an indium electrode in one corner. Devices were measured on the opposite edge of the coupon. Current density versus electric field (J–ξ) measurements were taken using an Agilent 4156C semiconductor parameter analyzer. The MOS devices were illuminated by visible light using an Osram Halogen 150-W, 21 V lamp. The light was transmitted through an optical cable. The distance between the source and the sample was approximately 3.8 cm.

III. RESULTS AND DISCUSSION

A. Identification of entropy stabilized form

Shown in Fig. 1 are growth per cycle (GPC) plots for each film. GPCs for ZrO_2 and Ta_2O_5 were determined to be 0.051 and 0.054 nm/cycle, respectively, comparable to previous reports.[23,24] For the $Zr_xTa_yO_z$ films, GPC was found to be 0.049 nm/ABC cycle, slightly lower than reported by Kukli *et al.*[19]

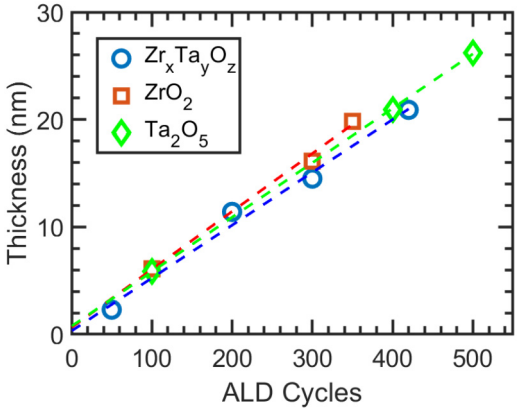

FIG. 1. GPC plots of thickness vs ALD cycle for Ta_2O_5 (green diamonds), ZrO_2 (red squares), and $Zr_xTa_yO_z$ (blue circles).

Shown in Fig. 2 are XRD scans of $Zr_xTa_yO_z$, Ta_2O_5, and ZrO_2 following postdeposition annealing at 800 °C in N_2 for 30 min. All films were amorphous as-deposited. Upon 800 °C annealing, the 19.8 nm thick binary Ta_2O_5 film crystallized into the hexagonal phase, while the 18.4 nm thick ZrO_2 film appeared to exhibit a mixture of the monoclinic and tetragonal phases. The 20.9 nm

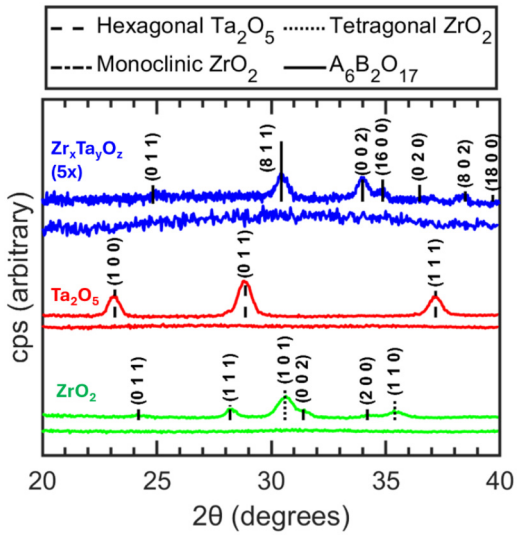

FIG. 2. Log XRD intensity (arbitrary units) vs 2θ of both as-deposited (bottom) and 800 °C annealed (top) for ZrO_2 (green), Ta_2O_5 (red), and $Zr_xTa_yO_z$ (blue, 5× scale). Vertical lines indicate the relative intensities and peak positions of $A_6B_2O_{17}$, 12 hexagonal Ta_2O_5 (PDF 19-1299), monoclinic ZrO_2 (PDF 86-1451), and tetragonal ZrO_2 (PDF 80-0965).

thick $Zr_xTa_yO_z$ film showed no overlap with any of the binary phase peaks. Instead, there was a close match of the peaks with those expected for the $A_6B_2O_{17}$ entropy stabilized phase family.[11,12] The overall intensities of the peaks in Fig. 2 are low, the full width half max is fairly broad, and not every $Zr_6Ta_2O_{17}$ peak is present, consistent with small crystallite sizes. The absence of the constituent binary peaks suggests that the Zr and Ta were well mixed, enabling the direct homogenous synthesis of solely the ESO phase.

Previous studies of $Zr_6Ta_2O_{17}$ formation in the bulk regime showed that though the initial phase formation temperature was generally consistent with predictions for a disordered system,[11] high temperatures and/or longer dwell times were required to achieve complete conversion of precursors to the $Zr_6Ta_2O_{17}$ ESO phase: 1300 °C for 10 h,[11,12] 950 °C for 24 h for a mixed phase with the pure $Zr_6Ta_2O_{17}$ phase after annealing at 1000 °C for 24 h,[6] and at ≥1400 °C for 12 h in air.[13] This is generally unsurprising, given the nature of solid-state synthesis for refractory species. For sputtered thin films, only a broad (811) peak was detected in the as-deposited films and postdeposition annealing was not performed.[14] Based on these studies, it is likely that annealing at a higher temperature for longer durations would allow for increased crystallization. Rapid thermal annealing of a separate film at 1100 °C for 1 min in N_2 (see Fig S1 in the supplementary material) showed broader and more intense (811) and (011) peaks at ~30.5° and ~25°, respectively, a broader (002) peak at 34°, and an additional peak at ~36°. It is likely that these differences are associated with the presence of binary ZrO_2 phases. Annealing for longer than 1 min at 1100 °C or at temperatures greater than 1100 °C was not possible with the equipment that was available. A film deposited with a 3:1 pulse ratio of $ZrCl_4$ to $Ta(OEt)_5$ and annealed at 800 °C showed only peaks associated with tetragonal ZrO_2 (see Fig. S2 in the supplementary material).

Another ternary phase with many similar peaks has also been reported. Bulk ternary $TaZr_{2.75}O_8$ ceramics formed by solid-state reaction at 1600 °C for 20 h showed similar peak positions (PDF No. 42-0060), but mixed with monoclinic ZrO_2.[20] For thin ZrO_2–Ta_2O_5 films deposited via ALD on 2 nm chemical oxide/(100)Si, a subset of the $A_6B_2O_{17}$ peaks seen in Fig. 2 was reported upon annealing for 30 min in N_2 at 800 °C and attributed to $TaZr_{2.75}O_8$.[19] In that work, an extra peak (likely monoclinic ZrO_2) was detected, indicating formation of a mixed phase. Note that these reports were prior to the original identification of the ESO $A_6B_2O_{17}$ family.

We previously investigated ternary $Hf_xTa_yO_z$ films deposited via ALD using different precursor chemistry [tetrakis(ethylmethylamido)hafnium (TEMAHf) and H_2O]. Upon annealing for 30 min in N_2 at 800 °C, those films showed only binary hexagonal Ta_2O_5. The $(A,B)_mO_{2m+1}$ ESO phase was not detected.[25] This is consistent with the predicted decomposition temperatures, below which the ternary ESO phase decomposes into the constituent binary phases: 875 ± 188 °C versus 627 ± 145 °C for $Hf_xTa_yO_z$ versus $Zr_xTa_yO_z$, respectively.[11]

RBS analysis on a 33 nm thick $Zr_xTa_yO_z$ film annealed at 800 °C revealed a two-layer structure with a 22 nm thick top layer consisting of approximately 13.6% Zr, 13.0% Ta, and 73.4% O (Zr:Ta = 0.97–1.13), and an 11 nm thick slightly Ta rich bottom layer consisting of approximately 12.9% Zr, 15.4% Ta, and 71.7% O (Zr:Ta = 0.78–0.90). $Zr_6Ta_2O_{17}$ is a member of a $(A,B)_mO_{2m+1}$ homologous series, where m = 8. Despite differences in composition, the members of this series have the same crystal structure due to the nature of stacked morphology consisting of 6, 7, and 8-coordinated polyhedral slabs where compositional changes are accommodated by increasing or decreasing the number of 7-coordinated slabs.[11] Members of the series also have the same configurational entropy per cation. Whereas the m = 8 and higher members are predicted to be thermodynamically favorable, the m = 4 and m = 6 are not, nor have they been previously reported.[11,12] The approximate 1:1 Zr:Ta ratio top layer indicated by RBS suggests that the $Zr_2Ta_2O_9$ (m = 4) homolog, only one 7-coordinated slab, was stabilized.[11,12] Though not thermodynamically favorable in bulk form, the presence of interfaces and the ability to cool more quickly may have helped to enable the formation of $Zr_2Ta_2O_9$ in thin film form. The difference in the crystal structure between the similarly processed ALD films in Kukli *et al.*[19] and those reported here could be due to less homogeneous mixing of metal ions, deposition on a chemical versus a native oxide, or a less rapid cooling rate following annealing.

B. Light-activated threshold voltage switching

Plots of J–ξ for as-deposited (amorphous) and 800 °C postdeposition annealed (crystalline/entropy stabilized) Ag/$Zr_xTa_yO_z$/Si MOS devices are shown in Fig. 3, both in the dark and under illumination. In the dark under positive bias, both as-deposited [Fig. 2(a)] and annealed [Fig. 2(b)] devices showed an "n"-shape (voltage-controlled) negative differential resistance (NDR),[26] with current density peaking at +0.72 and +0.41 MV/cm, respectively. NDR behavior has been previously reported in other MOS devices and attributed to multiple intervalley carrier transfer, defect assisted, or band based tunneling mechanisms.[27–29] The NDR behavior here may be caused by the filling of a high density of interfacial traps at the oxide/Si interface as the Fermi level rises through the bandgap under positive gate bias.[30] Assuming a distribution of trap energy levels at the Si/SiO_2 interface, the NDR current peak corresponded to the position at which the Fermi level was expected to be near the center of the Si bandgap.[25] It has been suggested that NDR followed by the onset of switching is an indication of filament formation involving oxygen vacancies.[31] However, no switching occurred within this voltage sweep range in the dark for either device.

Under illumination, NDR was no longer seen, swamped by the photogeneration of carriers in the Si. While the as-deposited amorphous devices did not show resistive switching within this sweep range [Fig. 3(a)], the annealed $Zr_2Ta_2O_9$ ESO devices [Fig. 3(b)] exhibited threshold voltage type resistive switching when illuminated under positive bias,[32–35] rapidly switching from the initial high resistance state (HRS) into the low resistance state (LRS) at a set field of ξ_{SET} = +0.56 MV/cm after which current saturates, limited by the supply of photogenerated carriers in the Si. Once in the LRS, exceeding a threshold field of ξ_{THRESH} = 0.18 MV/cm was required to show increased conduction (activate the low resistance).[35–38] In the dark, the LRS device could be reset by the application of a negative field at ξ_{RESET} = −0.84 MV/cm. Under illumination, ξ_{RESET} was reduced to −0.59 MV/cm.

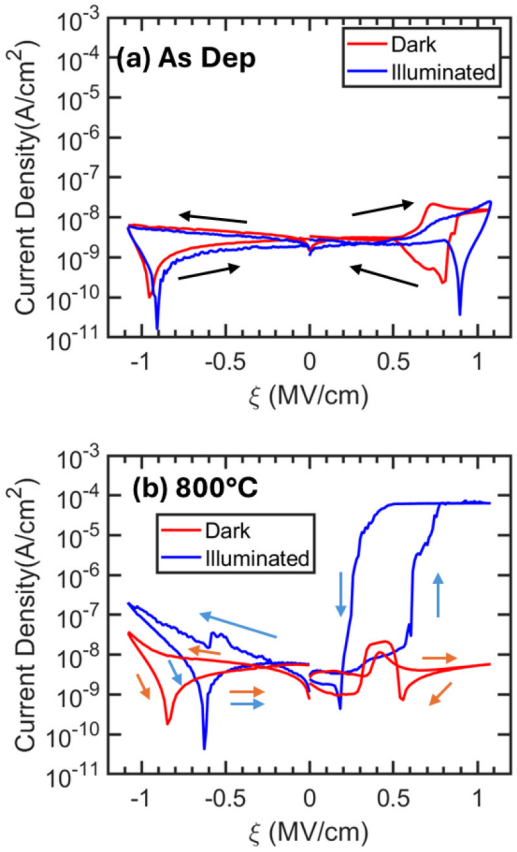

FIG. 3. Bipolar J vs ξ sweeps for (a) as-deposited and (b) 800 °C postdeposition annealed $Zr_xTa_yO_z$ devices in the dark/prior to illumination and under illumination.

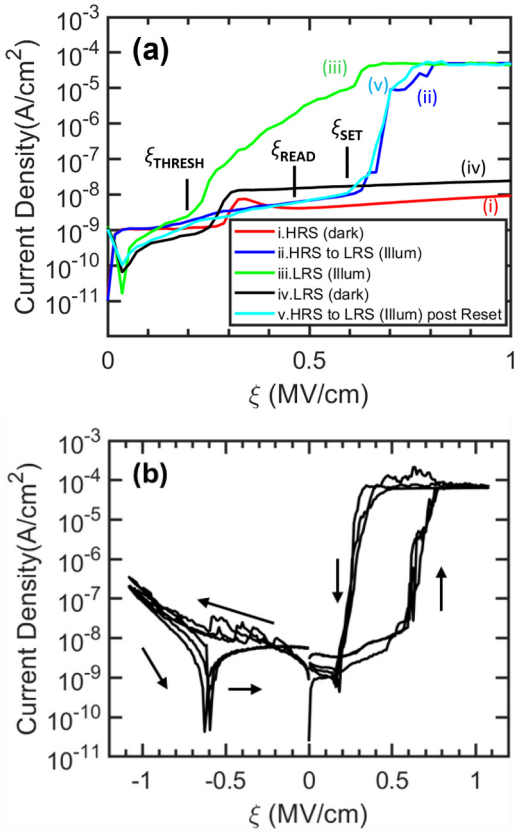

FIG. 4. (a) Positive polarity J–ξ sweeps illustrating each regime of device operation (described in the text) with the approximate set, read, and threshold fields indicated. (b) Three consecutive bipolar J–ξ sweeps under illumination showing repeated set and reset operations.

The series of sequential positive bias J versus ξ plots in Fig. 4(a) demonstrates device operation.

(i) Beginning in the dark, fresh devices were in the HRS.
(ii) During a following sweep under illumination, the current increased abruptly at $\xi_{SET} = +0.56$ MV/cm, setting the device to the LRS. The set operation occurred with the first positive bias sweep under illumination exceeding ξ_{SET}, without the need for a separate higher field forming sweep and external current compliance as is typically necessary for standard RRAM. Current is self-limited by the photogenerated carrier density.[32]
(iii) Now in the LRS, during subsequent positive bias sweeps under illumination, an abrupt increase in current took place when a minimum threshold field, $\xi_{THRESH} = 0.18$ MV/cm, was exceeded. The fact that ξ_{THRESH} was less than ξ_{SET} indicated that the device remained in the LRS. As opposed to standard metal oxide RRAM devices that show an immediate rise in current in the LRS, the ξ_{THRESH} requirement classifies this device as a *threshold* switching device.[35–39]
(iv) Subsequent sweeps in the dark demonstrated a small rise in current, near the peak of the initial NDR, that saturates, indicating that the device remained in the LRS without continuous illumination. Devices remained in the LRS until the application of a *negative* reset field (at least $\xi_{RESET} = -0.59$ MV/cm under illumination or -0.84 MV MV/cm in the dark) placed the device back in the HRS, indicating nonvolatility.
(v) Following a reset operation, the device remained in the HRS until a subsequent positive bias sweep under simultaneous illumination again exceeded $\xi_{SET} = +0.56$ MV/cm.

The separation between ξ_{THRESH} and ξ_{SET} allowed the device to be operated as a *self-rectifying* nonvolatile memory. As shown in Fig. 4(a), at a read field of $\xi_{READ} = +0.5$ MV/cm, the current density in the LRS and HRS was 1.1×10^{-8} and 6.2×10^{-5} A/cm^2, respectively, giving an LRS/HRS current ratio of $\sim 10^3$. Figure 4(b) shows three repeated set and reset operations while under illumination, demonstrating the basic repeatability of switching.

Standard (without ξ_{THRESH}) nonrectifying switching was also possible in the as-deposited amorphous devices under illumination, with a higher $\xi_{SET} = +1.6$ MV/cm. However, neither binary oxide device showed switching in this voltage range, either in the dark or under illumination. Kukli *et al.* saw standard resistive switching requiring a higher *negative* voltage forming step in amorphous as-deposited 20–35 nm thick Pt/Ta_2O_5:ZrO_2/TiN metal/insulator/metal (MIM) devices. Switching was suppressed by crystallization and, thus, not observed in their crystallized $TaZr_{2.75}O_8$ films.[19] Neither MOS devices nor light-activated switching were investigated.

C. Discussion of switching mechanisms

In previous reports on light-activated threshold switching in MOS structures, switching in ITO/SiO_2/Si MOS devices was attributed to the injection of photogenerated electrons in the Si leading to accelerated Si–O bond breaking and the formation of additional oxygen interstitials and V_O's at the Si/SiO_2 interface, reducing the formation voltage of conductive V_O filaments.[32,33,40] Light-activated switching of *opposite* polarity in Pd/Al_2O_3/SiO_2/Si MOS devices was attributed to electron trapping in Al_2O_3 and modulation of the depletion layer in Si due to injection of photogenerated electrons from Si and their removal from Al_2O_3 under negative bias. In Ag/$Hf_xTa_yO_z$/Si MOS devices (that were not crystallized in the ESO state), we attributed the light-activated threshold switching to the formation and dissolution of Ag^+ ion filaments, enhanced by injection of photogenerated electrons from the Si, with the threshold field due to the Schottky barrier at the Ag filament/Si interface.[25] In that study, illumination had no impact on MIM devices and Al gated MOS devices did not exhibit any switching phenomena. The light-activated threshold switching in the Ag/$Zr_2Ta_2O_9$/Si MOS devices here is likely due to a similar mechanism. For the unannealed $Zr_xTa_yO_z$ devices, the more gradual set response and lack of an ξ_{THRESH} suggests that the switching mechanism may be different. The gradual set behavior without a separate high field forming step may point to Schottky barrier modification, for example, in which oxygen vacancies gather or are removed near the interface.[41,42]

The observation of switching at lower fields in the annealed crystalline ESO ternary phase devices may be due to the higher metal ion diffusion rates, as previously reported for high entropy oxide (HEO) materials.[43] Increased ion mobility in the crystalline state over the amorphous state is not generally observed due to local crystal lattice distortions which lower overall ion mobility.[44,45] However, it has been demonstrated that local distortions in HEOs can give rise to increased ionic mobility.[46] This property has been exploited for battery applications in which HEOs have demonstrated orders-of-magnitude higher ionic conductivities.[43] In this work, increased ionic mobility in the crystalline $Zr_2Ta_2O_9$ ESO phase could have allowed for faster Ag^+ diffusion and facilitated conductive Ag filament formation as compared to the unannealed amorphous films, reducing the required switching fields.

IV. SUMMARY AND CONCLUSIONS

In this work, we have formed ternary entropy stabilized thin film zirconium tantalum oxide via ALD and subsequent postdeposition annealing. Amorphous as-deposited films crystallized into the entropy stabilized $(A,B)_mO_{2m+1}$ homologous series phase *without* the presence of binary phases upon annealing in N_2 at 800 °C, a much lower temperature than the ≥1300 °C typically required for stabilization of this phase family in bulk. Multiple XRD peaks were observed, all consistent with this ternary phase family. RBS analysis indicated an approximate Zr:Ta ratio of 1:1 suggesting stabilization of the $Zr_2Ta_2O_9$ (m = 4) homolog, the first time this has been reported.

ESO Ag/$Zr_2Ta_2O_9$/Si MOS devices showed light-activated self-rectifying threshold voltage. Under illumination and positive bias applied to the Ag electrode, devices were switched from an initial HRS to the LRS at $\xi_{SET} = +0.56$ MV/cm, *without* a separate electroforming step. Devices could not be set in the dark. A $\xi_{THRESH} = +0.18$ MV/cm was required in the LRS and an LRS/HRS current density ratio of 1.2×10^3 was found at $\xi_{READ} = +0.55$ MV/cm. The device could be reset from the LRS back to the HRS at $\xi_{RESET} = -0.59$ MV/cm under illumination or −0.84 MV/cm in the dark. Light-activated switching behavior was not seen in the amorphous form within the same ±1 MV/cm sweep range. The mechanism responsible for switching was likely Ag filament formation aided by enhanced Ag^+ mobility in the ESO phase and the injection of photogenerated electrons from the Si, with the threshold field potentially a result of a Schottky barrier at the Ag filament/Si interface.

Self-rectifying resistive switching with the absence of a high voltage electroforming step and the set current self-limited by photogeneration combined with ESO stabilization at relatively low temperature makes $Zr_2Ta_2O_9$ merit further investigation for applications such as low voltage high density selector-only crossbar memory arrays.[47]

SUPPLEMENTARY MATERIAL

The supplementary material contains two figures' additional data.

ACKNOWLEDGMENTS

The authors thank Chris Tasker and Rick Presley of Oregon State University for equipment support. This work was conducted at the Materials Synthesis and Characterization (MaSC) Center, a National Nanotechnology Coordinated Infrastructure (NNCI) Northwest Nanotechnology Infrastructure (NWNI) user facility at Oregon State University. This work was in part funded by an Unlock Ideas grant from Lam Research. Additional acknowledgments to the David C. Johnson Solid Sate Synthesis and Materials Research Group at the University of Oregon for allowing the use of their Rigaku Smart Lab XRD.

AUTHOR DECLARATIONS

Conflict of Interest

The authors have no conflicts to disclose.

Author Contributions

Shane M. W. Witsell: Conceptualization (lead); Data curation (lead); Formal analysis (lead); Investigation (lead); Methodology (lead);

Visualization (lead); Writing – original draft (lead); Writing – review & editing (equal). **Konner E. K. Holden:** Conceptualization (equal); Formal analysis (supporting); Methodology (supporting); Supervision (supporting); Writing – review & editing (supporting). **Dustin Z. Austin:** Conceptualization (equal); Formal analysis (supporting); Supervision (supporting); Writing – review & editing (supporting). **John F. Conley Jr.:** Conceptualization (equal); Formal analysis (equal); Funding acquisition (lead); Methodology (equal); Project administration (equal); Resources (equal); Supervision (equal); Validation (equal); Visualization (equal); Writing – original draft equal); Writing – review & editing (equal).

DATA AVAILABILITY

The data that support the findings of this study are available from the corresponding author upon reasonable request.

REFERENCES

[1]C. M. Rost, E. Sachet, T. Borman, A. Moballegh, E. C. Dickey, D. Hou, J. L. Jones, S. Curtarolo, and J.-P. Maria, Nat. Commun. **6**, 8485 (2015).
[2]S. S. Aamlid, M. Oudah, J. Rottler, and A. M. Hallas, J. Am. Chem. Soc. **145**, 5991 (2023).
[3]A. Salian and S. Mandal, Crit. Rev. Solid State Mater. Sci. **47**, 142 (2022).
[4]D. Bérardan, S. Franger, D. Dragoe, A. K. Meena, and N. Dragoe, Phys. Status Solidi RRL **10**, 328 (2016).
[5]D. Bérardan, S. Franger, A. K. Meena, and N. Dragoe, J. Mater. Chem. A **4**, 9536 (2016).
[6]R. J. Spurling, C. Skidmore, N. S. McIlwaine, and J.-P. Maria, J. Mater. Sci. **58**, 6164 (2023).
[7]H. Li *et al.*, Coatings **11**, 628 (2021).
[8]V. Jacobson, D. Diercks, B. To, A. Zakutayev, and G. Brennecka, J. Eur. Ceram. Soc. **41**, 2617 (2021).
[9]A. Sarkar *et al.*, Adv. Mater. **31**, 1806236 (2019).
[10]M. Brahlek *et al.*, APL Mater. **10**, 110902 (2022).
[11]A. A. Voskanyan, K. Lilova, S. J. McCormack, W. M. Kriven, and A. Navrotsky, Scr. Mater. **204**, 114139 (2021).
[12]S. J. McCormack and W. M. Kriven, Acta Crystallogr. B **75**, 227 (2019).
[13]Z. Y. Tan, G. Yan, K. Cao, C. Y. Cheng, L. Yang, and Y. C. Zhou, Ceram. Int. **49**, 29449 (2023).
[14]R. J. Spurling, S. S. I. Almishal, J. Casamento, J. Hayden, R. Spangler, M. Marakovits, A. Hossain, M. Lanagan, and J.-P. Maria, J. Am. Ceram. Soc. **107**, 19966 (2024).
[15]R. J. Spurling, M. T. Marakovits, A. Hossain, S. S. I. Almishal, S. E. Perini, M. T. Lanagan, and J.-P. Maria, Appl. Phys. Lett. **125**, 092901 (2024).
[16]J. Ferrand, V. Beugin, A. Crisci, S. Coindeau, S. Jeannot, M. Gros-Jean, and E. Blanquet, ECS Trans. **58**, 223 (2013).
[17]K. Kukli, J. Ihanus, M. Ritala, and M. Leskelä, J. Electrochem. Soc. **144**, 300 (1997).
[18]H. Zhang, R. Solanki, B. Roberds, G. Bai, and I. Banerjee, J. Appl. Phys. **87**, 1921 (2000).
[19]K. Kukli *et al.*, AIP Adv. **7**, 025001 (2017).
[20]J. Yuan, W. Song, H. Zhang, X. Zhou, S. Dong, J. Jiang, L. Deng, and X. Cao, Mater. Lett. **247**, 82 (2019).
[21]C. T. Nguyen, B. Gu, T. Cheon, J. Park, M. R. Khan, S.-H. Kim, B. Shong, and H.-B.-R. Lee, Chem. Mater. **33**, 4435 (2021).
[22]S. N. Chopra, M. F. J. Vos, M. A. Verheijen, J. G. Ekerdt, W. M. M. Kessels, and A. J. M. Mackus, J. Vac. Sci. Technol. A. **38**, 062402 (2020).
[23]K. Kukli, M. Kemell, J. Köykkä, K. Mizohata, M. Vehkamäki, M. Ritala, and M. Leskelä, Thin Solid Films **589**, 597 (2015).
[24]H. H. Sønsteby, V. A.-L. K. Killi, L. M. Rykkje, J. R. Bickford, E. G. Martin, R. C. Hoffman, and O. Nilsen, Dalton Trans. **51**, 927 (2022).
[25]S. M. Witsell, K. E. K. Holden, D. Z. Austin, and J. F. Conley, Jr., "Light-activated self-rectifying resistive switching in $Hf_xTa_yO_z$," AIP Adv. (submitted).
[26]B. K. Ridley, Proc. Phys. Soc. **82**, 954 (1963).
[27]R. Pant, N. Patel, K. K. Nanda, and S. B. Krupanidhi, J. Appl. Phys. **122**, 125303 (2017).
[28]G. Woo, T. Kim, and H. Yoo, Adv. Electron. Mater. **9**, 2201015 (2023).
[29]M. Dragoman and D. Dragoman, Solid State Electron. **197**, 108464 (2022).
[30]M. N. Getz, M. Povoli, and E. Monakhov, J. Appl. Phys. **129**, 205701 (2021).
[31]S. Saylan, H. M. Aldosari, K. Humood, M. Abi Jaoude, F. Ravaux, and B. Mohammad, Sci. Rep. **10**, 19541 (2020).
[32]M. Ungureanu, R. Zazpe, F. Golmar, P. Stoliar, R. Llopis, F. Casanova, and L. E. Hueso, Adv. Mater. **24**, 2496 (2012).
[33]A. Mehonic, T. Gerard, and A. J. Kenyon, Appl. Phys. Lett. **111**, 233502 (2017).
[34]O. Blázquez, J. L. Frieiro, J. López-Vidrier, C. Guillaume, X. Portier, C. Labbé, S. Hernández, and B. Garrido, Appl. Phys. Lett. **115**, 261104 (2019).
[35]G. Seo, B.-J. Kim, Y. Wook Lee, and H.-T. Kim, Appl. Phys. Lett. **100**, 011908 (2012).
[36]Y.-J. Huang, S.-C. Chao, D.-H. Lien, C.-Y. Wen, J.-H. He, and S.-C. Lee, Sci. Rep. **6**, 23945 (2016).
[37]Y. Choi, J. Shin, S. Moon, and C. Shin, Micromachines **11**, 525 (2020).
[38]Z. Wang *et al.*, Adv. Funct. Mater. **28**, 1704862 (2018).
[39]S. R. Ovshinsky, Phys. Rev. Lett. **21**, 1450 (1968).
[40]E. Mikheev, B. D. Hoskins, D. B. Strukov, and S. Stemmer, Nat. Commun. **5**, 3990 (2014).
[41]M. Hansen, M. Ziegler, L. Kolberg, R. Soni, S. Dirkmann, T. Mussenbrock, and H. Kohlstedt, Sci. Rep. **5**, 13753 (2015).
[42]S. Kumar *et al.*, Appl. Phys. Lett. **110**, 103503 (2017).
[43]B. Ran, H. Li, R. Cheng, Z. Yang, Y. Zhong, Y. Qin, C. Yang, and C. Fu, Adv. Sci. **11**, 2401034 (2024).
[44]K. A. Graeser, J. E. Patterson, J. A. Zeitler, and T. Rades, Pharmaceutics **2**, 224 (2010).
[45]E. Y. Pikalova, E. G. Kalinina, N. S. Pikalova, and E. A. Filonova, Materials **15**, 8783 (2022).
[46]Y. Zeng, B. Ouyang, J. Liu, Y.-W. Byeon, Z. Cai, L. J. Miara, Y. Wang, and G. Ceder, Science **378**, 1320 (2022).
[47]T. Ravsher *et al.*, IEEE Trans. Electron Devices **70**, 2276 (2023).